metals

MDPI

Article

Prediction of Fatigue Crack Growth in Vacuum-Brazed Titanium Alloy

Chou-Dian Huang [1], Jiun-Ren Hwang [1,*] and Jiunn-Yuan Huang [2]

[1] Department of Mechanical Engineering, National Central University, Taoyuan 320317, Taiwan; 106383011@cc.ncu.edu.tw
[2] National Atomic Research Institute, Taoyuan 325207, Taiwan; jyhuang@nari.org.tw
* Correspondence: jrhwang@ncu.edu.tw

Abstract: The assessment of fatigue is a crucial concern in welded components and structures. This study investigates the fatigue properties and models for predicting fatigue crack growth in Ti-6Al-4V titanium alloy when processed by vacuum brazing with TiCuNi filler. Fatigue properties and the impact of the stress ratio were determined through constant amplitude fatigue tests. By utilizing the results obtained from variable amplitude fatigue tests, various prediction models for fatigue crack growth were examined: modifications for load interaction, residual stress, and crack closure. The results indicate that the microstructures in the brazed zone consist of numerous fine, elongated needle-like Widmanstätten structures. In terms of cycle counting methods, the rainflow method outperforms the simple-range method. In the stable crack growth rate region, fatigue crack growth rate increases with the rise in stress ratio in a manner similar to high-strength steels. The Paris model without any modification obtains good predictions. For models modified with crack closure, the Elber model yields slightly better prediction results than the Schijve model. Among fatigue crack growth prediction models, the Willenborg model with residual stress modification produces the best results. Fracture surfaces within fatigued specimens' brazed zones exhibit ductile failure characteristics, where fatigue striations and secondary cracks were observed.

Keywords: vacuum brazing; titanium alloy; variable amplitude loading; fatigue crack growth evaluation

check for updates

Citation: Huang, C.-D.; Hwang, J.-R.; Huang, J.-Y. Prediction of Fatigue Crack Growth in Vacuum-Brazed Titanium Alloy. *Metals* **2023**, *13*, 1879. https://doi.org/10.3390/met13111879

Academic Editors: Francesco Iacoviello and Antonio Mateo

Received: 2 October 2023
Revised: 31 October 2023
Accepted: 9 November 2023
Published: 12 November 2023

Copyright: © 2023 by the authors. Licensee MDPI, Basel, Switzerland. This article is an open access article distributed under the terms and conditions of the Creative Commons Attribution (CC BY) license (https://creativecommons.org/licenses/by/4.0/).

1. Introduction

The excellent properties of titanium alloys have led to a significantly increased demand for them in the defense, aerospace, transportation, and biomedical industries. Titanium alloy welding has become an important manufacturing process in order for components and structures to meet the requirements of use. Vacuum brazing (a type of solid-state welding) is carried out in a vacuum environment of 1.33×10^{-1} to 1.33×10^{-4} N/m^2, without oxidation problems, and does not require the use of brazing flux. The joint surface has a metallic luster, and there are no post-weld cleaning or corrosion issues, which results in excellent joint quality [1].

The fatigue properties of welded structures are influenced by factors other than the machined components. For instance, in vacuum brazing, when the thickness of the specimen increases, the brazed contact area becomes larger, resulting in better joint strength and increased tensile strength. However, in the fatigue life assessment, the thickness modifications proposed by existing international standards such as Eurocode 3 [2], BS 7608 [3], and IIW [4] are not applicable; hence, the applicability of fatigue life prediction or fatigue crack growth should be re-evaluated.

Regarding the fatigue behaviors of Ti-6Al-4V joints, Balasubramanian et al. [5] investigated the fatigue crack growth behavior of Ti-6Al-4V after GTAW, EBW, and LBW welding. Guo et al. [6] studied TC4 using TIG welding and examined the impact of defect characteristics on fatigue life prediction. Liu et al. [7] explored the crack closure characteristics of a novel titanium alloy. Wang et al. [8] conducted research on the fatigue crack

growth behavior of TC2 using TIG welding. It can be observed that the test samples of the above studies are all fusion-welded. Vacuum brazing is a type of solid-state welding and is categorized as diffusion welding. The research on fatigue properties of vacuum-brazed titanium alloys is relatively limited. In addition, the focus of research on vacuum-brazed titanium alloys is usually on heterogeneous welding, new brazing material properties [9], or the element effects on microstructures [10]. There is very little research on the fatigue crack growth characteristics and life prediction of TC4 after vacuum brazing.

Prediction of the fatigue life of components and structures is crucial in both design and practical applications [11]. Fatigue life prediction via numerical simulation has been applied in many engineering fields, such as marine structures [12], semiconductor processing [13], the defense industry, and transportation [14]. Prediction involves factors such as loading conditions [15–17], microstructures of materials [18], type and size of the defects [19], and the load spectrum [14,20,21]. The development of the fatigue crack growth prediction method began in the 1960s, when Paris and Erdogan [22] identified three regions of the fatigue crack growth rate (da/dN); they found a power law relationship between stress intensity factor range (ΔK) and da/dN in the stable crack growth region (region II). The crack growth rate becomes unstable when entering region III, a process which can be described by the Forman equation [23].

Furthermore, fatigue crack growth in a material can be influenced not only by ΔK, but also by stress ratio (R), overload, residual stress, load sequence, crack closure effect, and other factors. For example, Wheeler [16] studied the hysteresis effect of crack growth rate after encountering overload loads under constant amplitude fatigue conditions. Willenborg [20] modified the hysteresis phenomenon of crack growth rate caused by compressive residual stress acting on the tip of the crack. The crack closure phenomenon [24] showed that the fatigue crack surface is still in a closed state, and the crack will not grow until a significant tensile load appears. In addition, Austen [25] studied the modification of the effective stress intensity factor range under constant amplitude load, considering both crack closure and static failure conditions. However, the above models are all based on homogeneous materials and are theoretical or semiempirical considerations. Moreover, the suitability of these modification models under variable amplitude loading, as well as in the case of welded structures, remains to be studied.

Therefore, the main objective of this study is to investigate the effects of mean stress and overload on fatigue crack growth of a vacuum-brazed titanium joint and to establish the optimal fatigue crack growth analysis model. The models under investigation are the traditional Paris model, Willenborg model, Elber model, Schijve model, and Austen model.

2. Materials and Methods

The Ti-6Al-4V alloy exhibits an excellent combination of high specific strength, corrosion resistance, and high-temperature properties. This alloy was utilized as the base material, with ribbon-shaped TiCuNi alloy serving as the filler material. Chemical compositions are listed in Table 1. The experimental procedure was as follows: The base metal plate was situated in a graphite jig, with the filler metal placed between the two base materials to form a butt weld specimen. The jig was secured and placed at the center of an upright vacuum furnace. Due to graphite's rapid and uniform heat conduction, as well as its low thermal expansion coefficient, it was utilized in place of a common metal jig. Using a graphite jig for vacuum brazing, the small contact area issue was overcome, thereby enabling successful completion of the thin plate joint. The vacuum brazing process parameters were the same as those of the previous study [26] and were optimized for the highest tensile strength. These included a soaking temperature of 890 °C, soaking time of 60 min, brazing temperature of 975 °C, and holding time of 45 min. Fatigue specimens were not subjected to heat treatment.

Table 1. Chemical compositions of the base metal and filler metal.

Material	Chemical Composition (wt.%)							
	Al	**V**	**Cr**	**Fe**	**Ni**	**Ti**	**Cu**	**Ni**
Ti-6Al-4V	5.88	3.60	0	0.08	0.08	Bal.	0	0
TiCuNi	0	0	0	0	0	70	15	15

In general, there were two samples for each test condition. The geometry of the specimen and groove is shown in Figure 1. As a result of the higher strength of the brazed bead material compared to the base metal, cracks cannot propagate straight along the weld bead. Therefore, grooves were machined on both sides of the specimen using electrical discharge machining (EDM). The grooves were made symmetrically at both sides of the specimen with a depth of 0.35 mm, an angle of 60 degrees, a radius of the groove tip of 0.2 mm, and a stress concentration factor of 3.1.

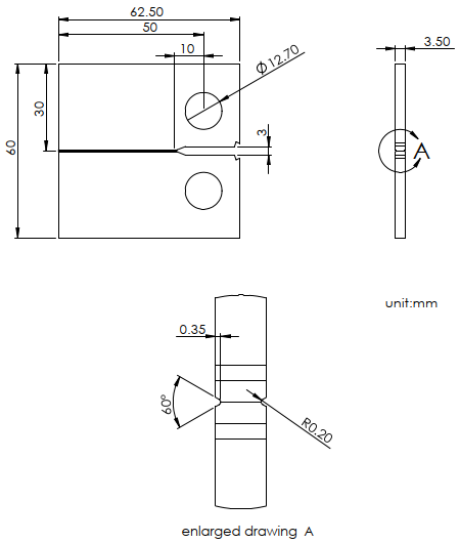


Figure 1. The geometry of the specimen and grooves.

After mounting, grinding, and polishing, the metallographic specimens were corroded by ASTM Kroll's Reagent for 15–25 s. Subsequently, they were cleaned and dried with water and alcohol. Observation of the microstructures was carried out at various positions, namely the brazed bead, heat affected zone, and base material.

The constant amplitude fatigue crack growth test was carried out in accordance with the ASTM E647 [27] standard. A compact tension specimen was adopted, and the experiment was performed using an MTS-810 universal material testing machine. Fatigue pre-cracking was executed with the decreasing stress intensity factor method. After pre-cracking, fatigue crack growth tests were conducted with sine wave loading of constant amplitude for various stress ratios, specifically 0.1, 0.3, and 0.5. The selection for R ratios of 0.1, 0.3 and 0.5 was to observe the effect of the stress ratio on the fatigue crack growth rate.

The pre-cracking method for the variable load amplitude test was the same as that for the constant load amplitude test. The loading histories, comprising transmission (TRN), bracket (BRK), and suspension (SUS) histories, were provided by the Society of Automotive Engineers (SAE).

In order to accelerate the experiment, the insignificant smaller loadings in original histories were eliminated with the trajectory tracking method [28], with track width 56% (for TRN and BRK) and 31% (for SUS). The data points of the reduced TRN, BRK, and SUS histories were 103, 313, and 151, respectively. Furthermore, in order to facilitate smooth action of the hydraulic actuator, the data points of BRK and SUS histories were increased to 414 and 211, respectively, by interpolation. These histories were shown in Figure 2. The

simplified load history was further adjusted to achieve the specified maximum load and a minimum-to-maximum stress ratio (R_v) of 0.1, and the output rate of *D/A* (loading) was 10 Hz in the fatigue test.

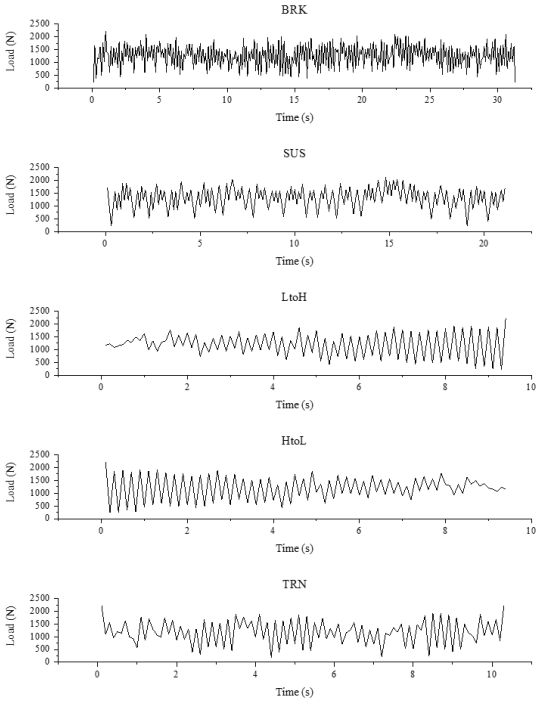


Figure 2. Variable load amplitude histories.

To understand the load sequence effect, the load cycles in the TRN history were extracted with the rainflow method [28] then reassembled according to the order of the stress ratio. Two load histories were obtained, as shown in Figure 2. One is sorted from low to high stress ratio and is called HtoL; the order of stress amplitude is roughly from large to small. The other history, with a stress ratio from high to low, is called LtoH.

The crack length was measured using the crack opening displacement (COD) method specified in the ASTM E647 standard. The stress intensity factor range and normalized crack length (α) were calculated using Equations (1)–(4):

$$\Delta K = \frac{\Delta P}{\sqrt{BB_N w}} \frac{(2+\alpha)}{(1-\alpha)^{\frac{3}{2}}} \left(0.866 + 4.64\alpha - 13.32\alpha^2 + 14.72\alpha^3 - 5.6\alpha^4\right) \quad (1)$$

$$\alpha = \frac{a}{W} = 1.0012 - 4.9162 \times U_x + 23.057 \times (U_x)^2 - 323.91 \times (U_x)^3 + 1798.3 \times (U_x)^4 - 3513.2 \times (U_x)^5 \quad (2)$$

$$U_x = \left\{ \left[\frac{EVP}{P} \right]^{\frac{1}{2}} + 1 \right\}^{-1} \quad (3)$$

$$0.2 \leq a/w \leq 0.975 \quad (4)$$

where ΔP is the load range ($P_{max} - P_{min}$), B is the specimen thickness, B_N is the net thickness of the specimen, a is the crack length, W is the width of CT specimen, E is the modulus of elasticity, V is the COD value, and P is the load.

Fracture surfaces were examined after fatigue test. If the defect existed at the fracture surface or the crack propagation did not along the brazed region, the test results were discarded.

2.1. Method of Fatigue Crack Growth Prediction

The fatigue crack growth of vacuum-brazed Ti-6Al-4V joints was evaluated with TRN, BRK, and SUS load histories, respectively. Each history was considered as a block.

The fatigue crack growth and fatigue life were predicted with the block loading method [29], in which the crack growth per loading block $\Delta a/\Delta B$ was determined, instead of calculating crack growth by summing growth for each cycle. Two assumptions are made: (1) the actual loading history can be modeled by a repeating block of loading; (2) crack length is fixed during a loading block ($\Delta a/\Delta B << a$).

The change in crack length per block was calculated through the following steps:

1. The effective load range at the i^{th} loading cycle $(\Delta P_{eff})_i$ was determined using one of the following two methods: (1) Only tensile loads cause crack extension; if $P_{min} < 0$, let $P_{min} = 0$. (2) If crack closure load, P_{cl}, is considered and it is greater than zero, then

$$(\Delta P_{eff})_I = (P_{max})_i - (P_{cl})_i \tag{5}$$

2. $(\Delta K)_i$ or $(\Delta K_{eff})_i$ was determined with Equation (1) or according to a specific prediction model.
3. The increment of crack length per cycle was determined using the Paris equation:

$$\Delta a_i = \left(\frac{da}{dN}\right)_i = C(\Delta K)_i^m \tag{6}$$

In the Elber, Schijve, static fracture, Austen, Forman and Willenborg models, the increment of crack length per cycle was determined with the modified equation:

$$\Delta a_i = \left(\frac{da}{dN}\right)_i = C_0\left(\Delta K_{eff}\right)_i^m \tag{7}$$

where C_0 and m are material constants. C_0 and ΔK_{eff} correspond to the same closure level.

4. The change in crack length per block, $\Delta a/\Delta B$, was calculated. This was obtained by summing the change in crack length due to each loading cycle, i.

$$\frac{\Delta a}{\Delta B} = \sum_{i=1}^{n} \Delta a_i \tag{8}$$

where n is the number of cycles per block. Then,

$$\frac{\Delta a}{\Delta B} = \sum_{i=1}^{n} C_0\left(\Delta K_{eff}\right)_i^m \tag{9}$$

5. The crack length after p loading blocks, a_{p+1}, was determined,

$$a_{p+1} = a_p + \left(\frac{\Delta a}{\Delta B}\right)_p \tag{10}$$

6. The blocks to failure, B_f, were calculated,

$$B_f = \int_{a_i}^{a_f} \frac{\Delta B}{\Delta a} da \tag{11}$$

where the critical crack length a_f was obtained from the fracture toughness, which was 82 MPa$\sqrt{\text{m}}$ [30] in this study.

Various fatigue crack growth prediction models were programmed using Visual Basic 6.0. The simplified TRN, BRK, and SUS load histories were cycle-counted using the simple-range counting method [31] or the rainflow method [28]. Calculation of cumulative crack length was carried out using Equations (6)–(11), i.e., summation of crack increments. Crack growth for each block was estimated by considering the crack closure, overload loading, and static fracture modifications.

In Step 2, the value of ΔK_{eff} can be modified according to specific theories: namely, the Willenborg model, crack closure model, static fracture model, and the Austen model.

2.2. Willenborg Model

The Willenborg model is based on the assumption that crack growth retardation is caused by compressive residual stresses acting on the crack tip. At the i^{th} loading cycle, the compressive stress, $(\sigma_{comp})_i$, due to the elastic body surrounding the overload, is the difference between the maximum stress and the corresponding value of the required stress. The required stress is calculated on the basis that the boundary of the produced yield zone just touches the overload plastic zone boundary. The actual maximum and minimum stress at the i^{th} loading cycle are:

$$(\sigma_{max}{}^{e})_i = (\sigma_{max})_i - (\sigma_{comp})_i \tag{12}$$

$$(\sigma_{min}{}^{e})_i = (\sigma_{min})_i - (\sigma_{comp})_i \tag{13}$$

If either of these effective stresses is less than zero, it is set as equal to zero. The effective stress at the i^{th} loading cycle, $\sigma_i{}^{e}$, is:

$$\Delta\sigma_i{}^{e} = (\sigma_{max}{}^{e})_i - (\sigma_{min}{}^{e})_i \tag{14}$$

Then, the effective load can be obtained, and the effective stress intensity factor range at the i^{th} loading cycle is calculated using Equation (1).

2.3. Crack Closure Model

When the tensile stress around the crack tip exceeds the yield strength of the material, a plastic zone forms, causing crack closure. In the crack closure model [32], the stress intensity factor range is modified. The effective stress intensity factor range ΔK_{eff} is:

$$\Delta K_{eff} = U\Delta K \tag{15}$$

In the Elber model [32]:

$$U = 0.5 + 0.4R \tag{16}$$

In the Schijve model [33]:

$$U = 0.55 + 0.35R + 0.1R^2 \tag{17}$$

where R is the stress ratio.

2.4. Static Fracture Model

The growth rate of cracks increases as the length of cracks increases [34]. When the K_{max} approaches fracture toughness K_c, static failure is generated due to dimples of ductile or cleavage mechanisms and results in an increase in the crack growth rate. In order to predict the accelerated growth near the final failure, an additional K_{fs} value was introduced into the effective maximum stress intensity factor. The corresponding equations were:

$$\Delta K_{eff} = \Delta K_{maxeff} - \Delta K_{mineff} \tag{18}$$

$$\Delta K_{maxeff} = K_{max} + K_{fs} \tag{19}$$

$$K_{fs} = \frac{K_{max}}{(K_c - K_{max})} \tag{20}$$

where K_c is fracture toughness, and K_{fs} is static fracture intensity factor. From Equation (20), it can be seen that K_{fs} increases apparently as K_{max} approaches K_c. This modification by introducing fracture toughness K_c into the static fracture model is similar to that in the Forman equation [23].

2.5. Austen Model

The Austen model [25] accounts for both the crack closure and static fracture. The effective stress intensity factor range is calculated using Equations (21)–(23):

$$\Delta K_{eff} = K_{max,eff} - K_{min,eff} \tag{21}$$

$$\Delta K_{max,eff} = K_{max} + K_{fs} - K_R \tag{22}$$

$$\Delta K_{min,eff} = K_{min} \ \ or \ K_{cl} \tag{23}$$

where K_R is the residual stress intensity factor and K_{cl} is closure stress intensity factor. The original K_R was proposed by Willenborg. Austen extends the above formula to account for hysteresis and overload effects, giving K_R as in Equation (24).

$$\begin{array}{c} K_R = Z_{OL}[1 - \Delta a/(Z_{OL} - Z_i)]^{0.5} - (K_{OL} - K_{max}) \cdot (1 - \Delta a/Z_{rev})^{0.5} \\ -K_{max}(1 - \Delta a/Z_{OL})^{0.5} \end{array} \tag{24}$$

where Z_i is the maximum plastic zone size at the i^{th} loading cycle, Z_{OL} is the overload plastic zone size, and Z_{rev} is the reversed plastic zone size due to overload.

$$Z = (K_{max}/\sigma_y)^2/3\pi \tag{25}$$

$$Z_{OL} = (K_{OL}/\sigma_y)^2/3\pi \tag{26}$$

$$Z_{rev} = [(K_{OL} - K_{min})/\sigma_y]^2/12\pi \tag{27}$$

3. Results

3.1. Microstructures and Tensile Strength

The microstructure of the base material after vacuum brazing was quite similar to the original material, as shown in Figure 3a. It mainly consisted of white granular α-titanium, elongated β-titanium, and a layered structure formed by the alternating arrangement of α and β phases. The brazed zone exhibited a dark and elongated microstructure, as seen in Figure 3b. It was observed that the brazing filler material had completely melted. The average ultimate tensile strength was 1265 MPa, with the fracture located in the brazed bead [26]. The ultimate tensile strength exceeded those of the base material, laser beam weldment (LBW), and tungsten inert gas (TIG) weldment [26].

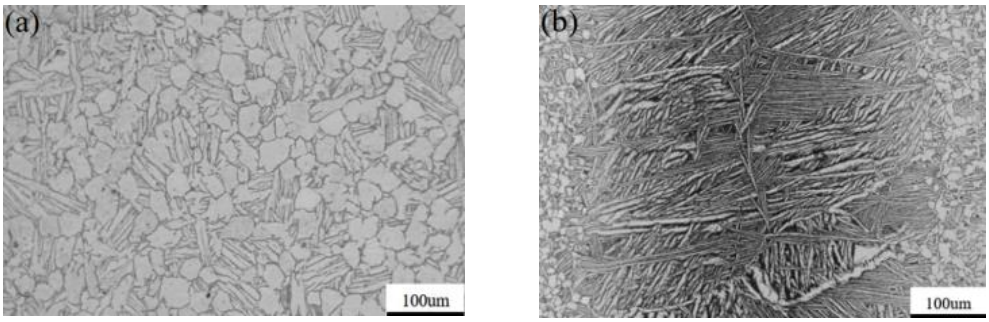


Figure 3. Microstructures. (**a**) Base metal and (**b**) brazed zone.

3.2. Fatigue Crack Growth Rate under Constant Amplitude Loading

Fatigue crack growth rates of the brazed zone for different stress ratios are shown in Figure 4. It can be seen that in the stable fatigue crack growth rate region, the fatigue crack growth rate increases with the rise in stress ratio. This indicates that the higher the stress ratio or mean stress, the greater the fatigue damage to the material in vacuum-brazed Ti-6Al-4V alloy. Sullivan [35] indicates that the *da/dN* increases with *R* at a fixed ΔK in high-strength steel. This observation is consistent with our experiment.

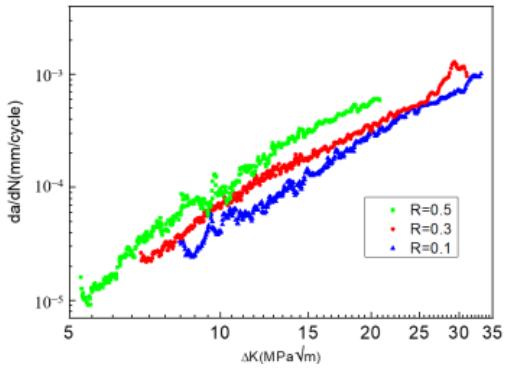


Figure 4. Influence of stress ratio on fatigue crack growth.

In Figure 5, a comparison is made between the *da/dN*-ΔK curves obtained in this experiment and those reported by Balasubramanian [5]. The self-welding GTAW, EBW, and LBW produce similar slopes in *da/dN*-ΔK curves. The order of crack growth rate is GTAW > EBW > LBW. However, in this experiment, due to the use of hard brazing filler with different chemical compositions from the base material, the slope is different. The crack growth rate is between those of GATW and LBW. The coefficients in the Paris equation are $C = 4.16 \times 10^{-8}$ and $m = 2.96$ for a stress ratio of 0.1 in this study.

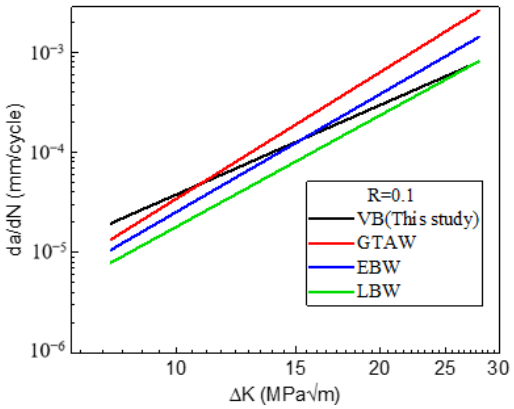


Figure 5. Influence of welding method on fatigue crack growth [5].

Figure 6 depicts the plotting of *da/dN* vs. ΔK_{eff} using the Elber and Schijve modifications; it is an experimental result with effective stress intensity factor range (ΔK_{eff}) as the label of the horizontal axis. The value of ΔK_{eff} was calculated using Equations (15) and (16) in the Elber model and using Equations (15) and (17) in the Schijve model. As shown in Figure 6a, the influence of the stress ratio can be effectively modified with the Elber model, i.e., Equation (16). The Schijve model exhibits a slightly worse modification than the Elber model, as shown in Figure 6b.

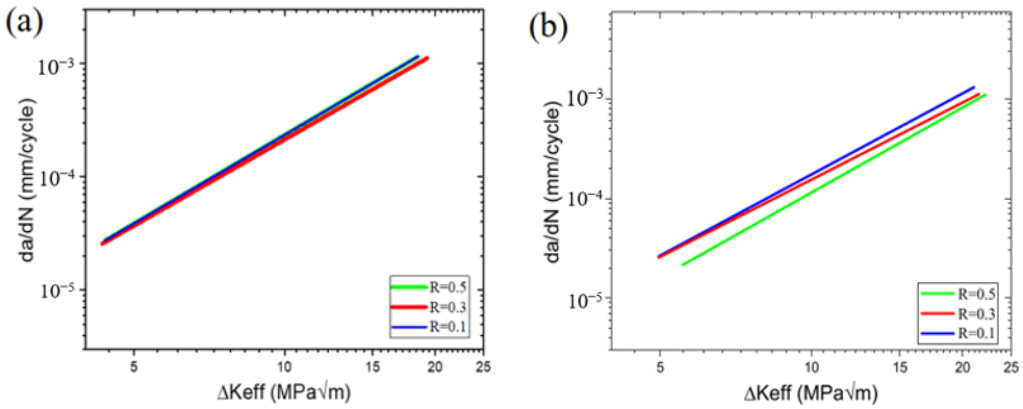


Figure 6. Influence of ΔK_{eff} on fatigue crack growth. (**a**) Elber model and (**b**) Schijve model.

3.3. Fatigue Crack Growth Rate under Variable Amplitude Loading

To investigate the effects of load interaction [17], three standard load histories were adopted: the transmission (TRN), bracket (BRK), and suspension (SUS) histories. Their characteristics are as follows: TRN had an abrupt change in the mean load, BRK had an almost constant mean load (or narrow-band random vibration), and SUS had a history with large variations at the beginning and end quarter sections but with a nearly constant mean load and small amplitude differences in the middle section.

Figure 7 shows the crack length vs. block number in the Ti-6Al-4V vacuum-brazed joints with the TRN, BRK, and SUS loading histories. The fatigue lives are 2406, 1314, and 6059 blocks for the TRN, BRK, and SUS loading, respectively.

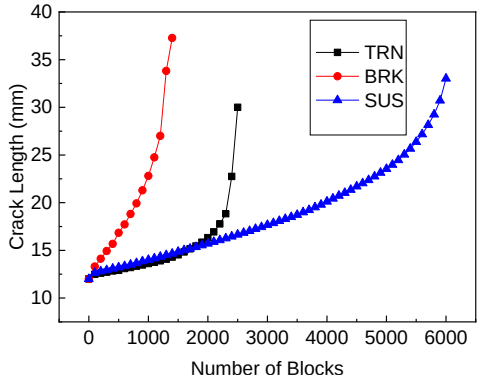


Figure 7. Experimental fatigue crack growth curves.

3.4. Prediction of Fatigue Crack Growth

Fatigue crack growth was predicted by various models. The codes of the fatigue analysis models are shown in Figure 8.

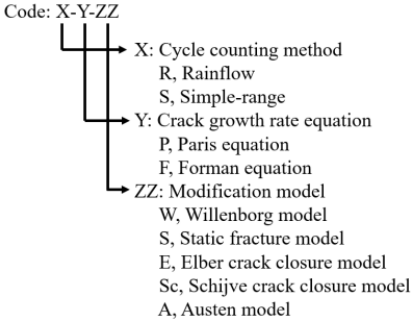


Figure 8. Code of fatigue analysis model.

3.4.1. Transmission, Bracket, and Suspension Histories

The fatigue crack growth of vacuum-brazed Ti-6Al-4V joints was predicted with TRN, BRK, and SUS load histories, respectively. This was carried out to investigate the influence of different characteristics of loading history on the crack growth. Each history was considered as a block because compressive load could transmit through the crack surface and result in the absence of stress concentration at the crack tip. It could not induce crack growth; thus, the loading history was shifted to the tensile region, and the ratio of minimum load to the maximum load, R_v, was set to 0.1. The maximum load was set to 3340 N. The experimental results are presented in Table 2.

Table 2. Experimental fatigue lives.

History	P_{max} (N)	P_{min} (N)	Fatigue Life (Blocks)
TRN	3340	334	2406
BRK	3380	338	1314
SUS	2565	256	6059

Figure 9 shows the effect of the cycle counting method on the fatigue prediction. It can be seen that the predicted life of the simple-range method is longer than the experimental value with these three histories; among them, the predicted life in the SUS history has the largest deviation. The predicted life of the rainflow method is closer to the experimental life; therefore, this cycle counting method is used in the subsequent analysis.

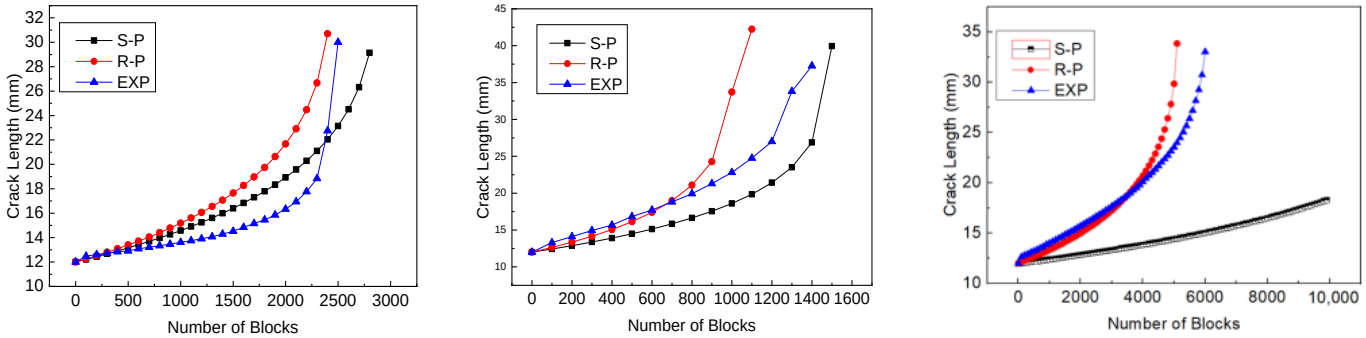


Figure 9. Effect of cycle counting method on fatigue crack growth curve. (**a**) TRN, (**b**) BRK, and (**c**) SUS.

Regarding the crack closure modification, Figure 10 shows a comparison of the results of the Paris, Elber, and Schijve models. It is evident that the prediction by the Paris model is closer to the experimental data, while the Schijve model shows the largest deviation. The Elber model yields slightly better prediction results than the Schijve model. The modification of crack closure models was less pronounced in the vacuum-brazed specimen with these standard loading histories.

Among three variable-amplitude loadings, the predicted life for the SUS history exhibits the largest deviation, probably due to the characteristics of the loading history. The SUS loading history has relatively small amplitude variations and is nearly constant in the middle section, making the influence of crack closure effects negligible.

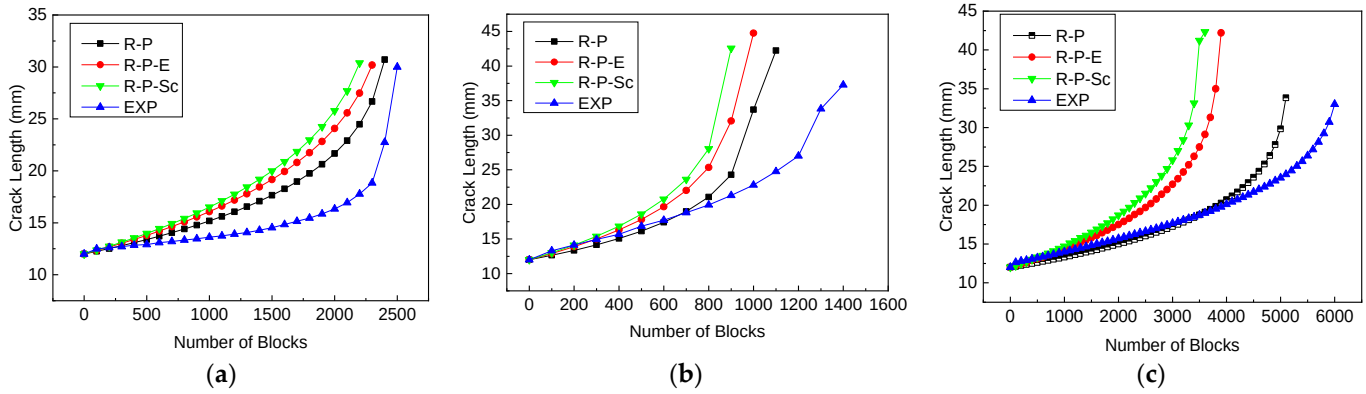


Figure 10. Effect of crack closure modification on fatigue crack growth curve. (**a**) TRN, (**b**) BRK, and (**c**) SUS.

Figure 11 shows a comparison of the Paris model, static fracture model, and Austen model. The static fracture model addresses the modification of crack growth in the higher crack growth rate region. Because the ΔK_{eff} is higher than ΔK, it predicts a shorter fatigue life than the Paris model. On the other hand, the Austen model accounts for the acceleration of crack growth in the later stages, along with an additional consideration of crack closure. The Austen model predicts a longer fatigue life than the Paris model. Among these three models, the result of the static fracture model is too conservative, while the Paris and Austen models have their own advantages and disadvantages.

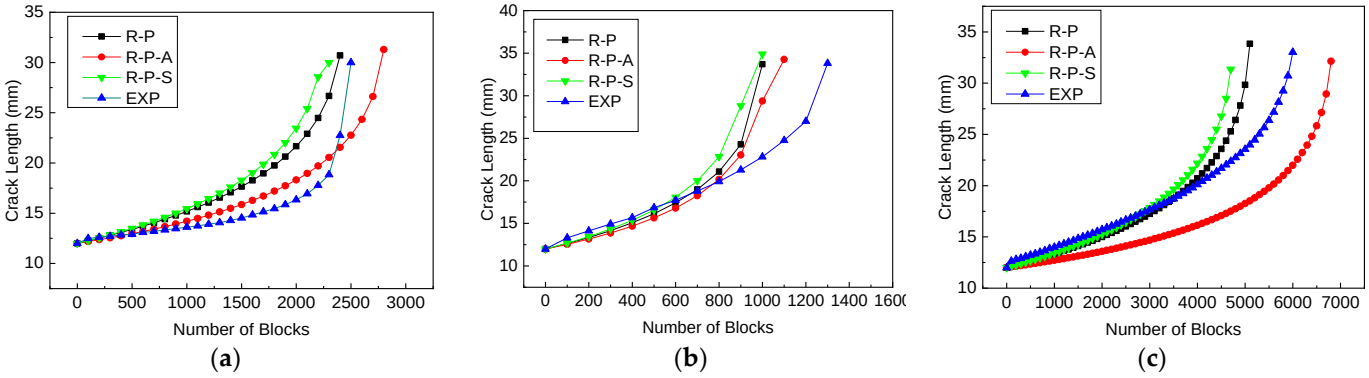


Figure 11. Effect of static fracture model and Austen model on fatigue crack growth curve. (**a**) TRN, (**b**) BRK, and (**c**) SUS.

The features of loading history affect the applicability of the prediction model. The characteristics of TRN, BRK, and SUS histories were described in Section 3.3. Regarding the Austen model, with the TRN loading history, the increase in fatigue life due to crack closure was more significant than the decrease in fatigue life caused by late-stage crack growth. With the BRK loading history, both static fracture and crack closure effects needed to be considered. However, with the SUS loading history, if the Austen model is used with simultaneous consideration of crack closure and static fracture effects, the predicted results would overestimate the fatigue life of the specimens.

In Figure 12, a comparison is made between the Paris model and Forman model. The latter was developed to model unstable crack growth (Region III) behavior, although it is more often used to model mean stress effects. This equation predicts the sharp upturn in the *da/dN* versus ΔK curve as fracture toughness is approached. From Figure 12a, it can be observed that the predictions from the Forman model deviate significantly from the experimental results. If the Forman model were used directly to assess the fatigue life of materials, it would produce unrealistically long fatigue life predictions in the early stage of

crack growth, due to the smaller K values. Only when the K value is sufficiently large can the Forman model adequately describe the crack growth behavior.

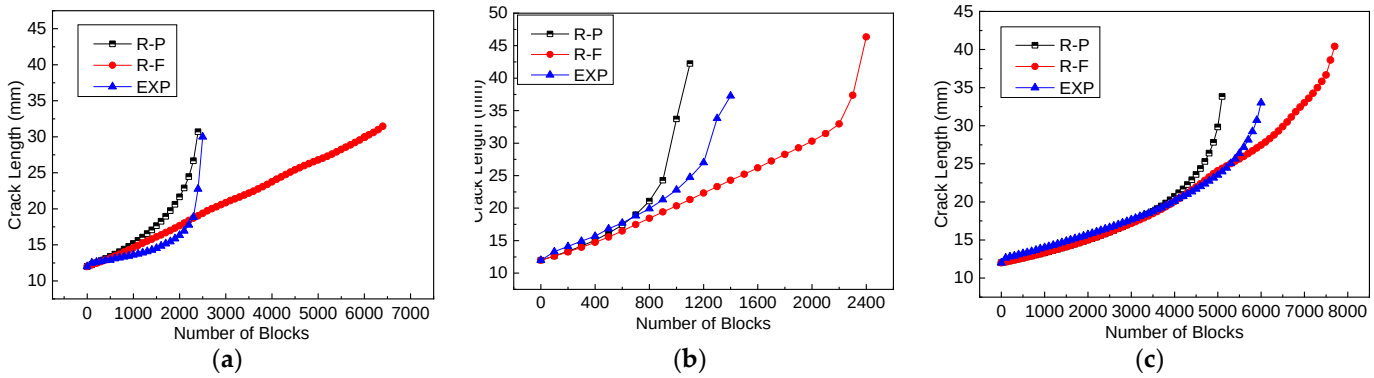


Figure 12. Fatigue crack growth curve of Forman model. (**a**) TRN, (**b**) BRK, and (**c**) SUS.

In Figure 13, the results of the Paris and Willenborg models are compared. The Willenborg model is based on the assumption that crack growth retardation is caused by compressive residual stresses acting on the crack tip. This model uses an effective stress, which equals the applied stress reduced by the compressive residual stress, to determine the effective stress intensity factor.

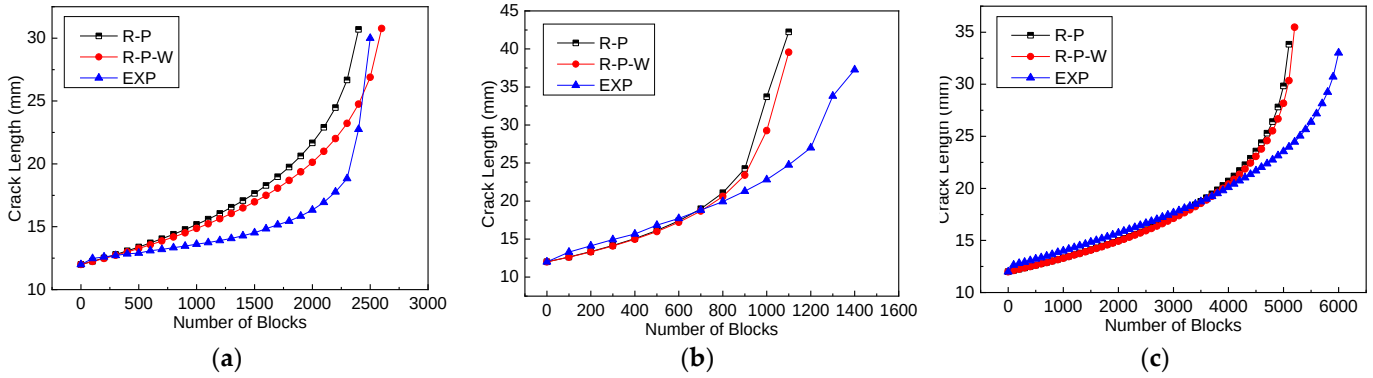


Figure 13. Fatigue crack growth curve of Willenborg model. (**a**) TRN, (**b**) BRK, and (**c**) SUS.

The Willenborg model predicts slightly slower crack growth and longer fatigue life than the Paris model. Its predictive results are closer to the experimental data for the TRN, BRK, and SUS histories. In addition, it is found that the Willenborg model produces the best results among all the prediction models in this study.

3.4.2. Load Sequence Effect

Load interaction effects on the fatigue crack growth were first recognized [35,36] in the early 1960s. The application of a single overload will cause a decrease in the crack growth rate, and its effect remains for a period of loading after the overload. Figure 14 shows a comparison of the TRN, HtoL, and LtoH histories; it reveals that the sequence effect indeed influences the fatigue life of the specimens. It is important to keep in mind that the abbreviation HtoL means that the sequence of load amplitude is roughly from large to small. The larger stress in the early stages of the HtoL history produces residual compressive stress field and increases the fatigue life. The fatigue life of the HtoL loading history is longer than that of the TRN history.

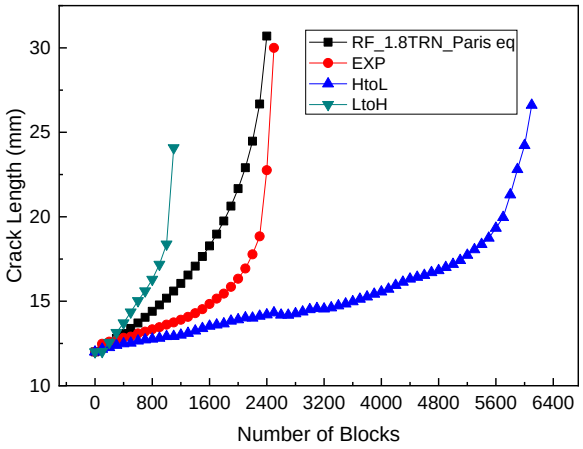


Figure 14. Effect of load sequence on fatigue crack growth curve.

Beden et al. [37] investigated the effect of the stress ratio and load sequence on the fatigue life by using six different load histories. In their study, case 1 involves a sequence of low-to-high stress amplitudes (similar to the LtoH history in this study), while case 2 involves a sequence of high-to-low stress amplitudes (similar to the HtoL history in this study). Based on Beden's results, it was found that the fatigue life in case 1 is lower than that in case 2. Their experimental results are consistent with those of this study. This indicates that the load sequence within a block does influence the fatigue life. As mentioned in the literature [37], the first larger tensile stress produces an overload effect on the material, and the resulting residual compressive stress field leads to a decrease in the effective stress of the subsequent loading, which reduces the crack growth rate and increases the fatigue life. On the contrary, with the LtoH loading history, the overload effect is smaller, and the fatigue life of the specimens is shorter than that of the TRN history.

3.5. Fractography

Fatigue failure can be divided into three stages: crack initiation, crack propagation, and rapid fracture. In the fracture surfaces of the specimens subjected to TRN, BRK, or SUS loadings, fatigue striations were observed in the crack propagation zone, and ductile dimples appeared in the rapid fracture zone as shown in Figures 15 and 16. Specimens subjected to cyclic loading with highly variable amplitude (TRN history) tend to have a more evenly distributed dimple/fibrous microstructure on the fracture surface, compared to those subjected to nearly constant amplitude (BRK history).

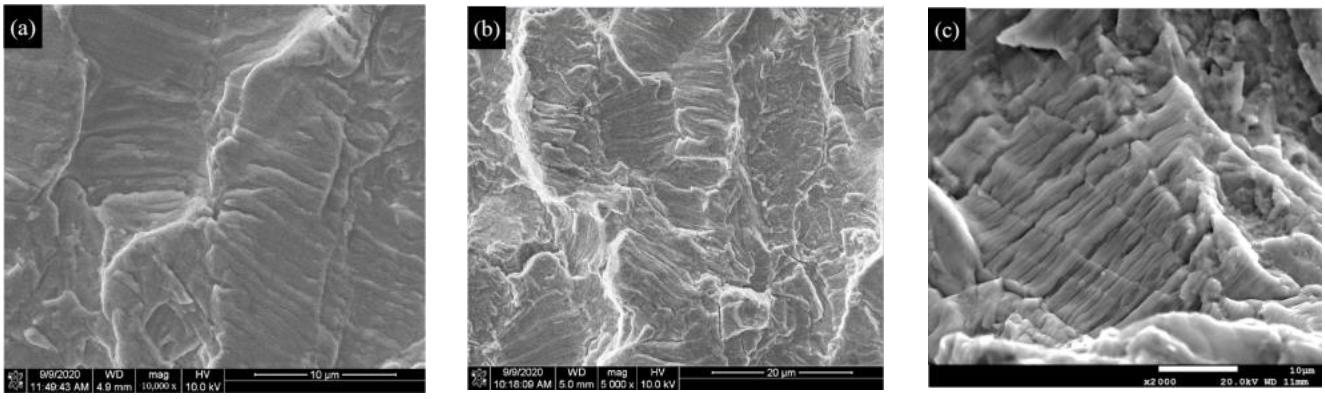


Figure 15. Fractographs in the crack propagation zone. (**a**) TRN, (**b**) BRK, (**c**) SUS.

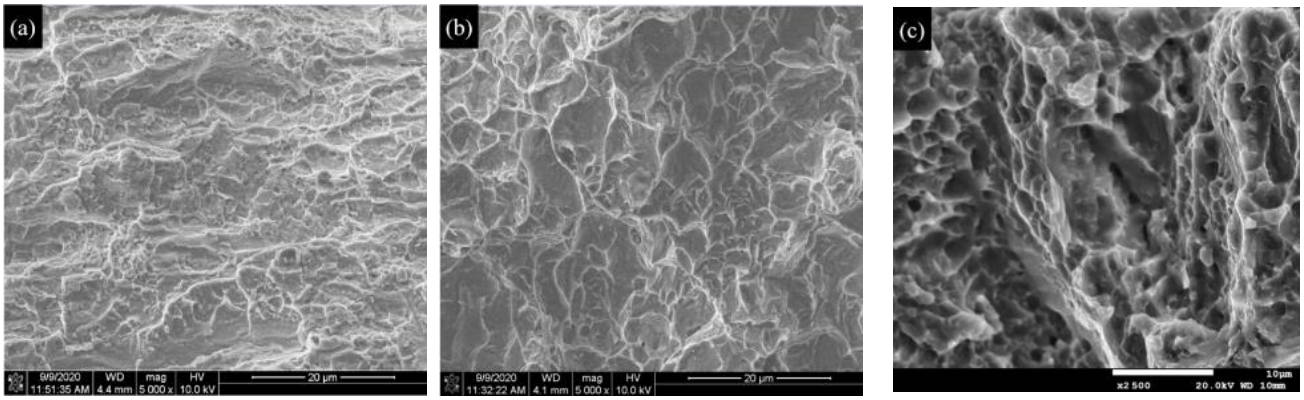


Figure 16. Fractographs in the rapid fracture zone. (**a**) TRN, (**b**) BRK, (**c**) SUS.

4. Conclusions

This study investigated fatigue properties and models for predicting fatigue crack growth in vacuum-brazed Ti-6Al-4V joints. Based on the results, the following conclusions can be drawn.

- In utilizing TiCuNi filler and an optimal vacuum brazing process, the microstructures of the base metal consisted of white, granular α-titanium, elongated β-titanium, and a layered structure composed of interwoven α and β phases. In the brazed zone, numerous fine, elongated needle-like Widmanstätten structures were observed, with no apparent cracks or defects on either side of the weld.
- During the stable crack growth stage (Region II), the higher the stress ratio, the greater the fatigue crack growth rate. The trend is similar to that found in steels.
- The rainflow cycle counting method outperforms the simple-range cycle counting method.
- The Paris model without any modification can obtain a good prediction.
- Regarding crack closure modification, the Elber model yields slightly better predictive results than the Schijve model.
- Among all fatigue crack growth prediction models, the Willenborg model, which accounts for residual stress modification, produces the best and most conservative results.
- When considering the load sequence effect, the load history reassembled with larger tensile load in the early stages results in lower effective stress of the subsequent loading and leads to higher fatigue life.
- Fracture surfaces at fatigue propagation zone of the vacuum-brazed Ti-6Al-4V joint exhibited ductile fracture characteristics, where fatigue striations were observed.

Author Contributions: Conceptualization, J.-R.H. and C.-D.H.; methodology, J.-R.H. and C.-D.H.; software, C.-D.H.; validation, C.-D.H.; investigation, C.-D.H.; resources, J.-Y.H.; data curation, C.-D.H. and J.-Y.H.; writing—original draft preparation, C.-D.H.; writing—review and editing, J.-R.H. and C.-D.H.; supervision, J.-R.H. All authors have read and agreed to the published version of the manuscript.

Funding: National Science and Technology Council, R.O.C. under the contract No. MOST 107-2221-E-008-071.

Data Availability Statement: Data are contained within the article.

Conflicts of Interest: The authors declare no conflict of interest.

Nomenclature

a	crack length
B	thickness of specimen
C	constant of Paris equation
C_0	reference compliance
E	Young's modulus
K	stress intensity factor
K_C	critical stress intensity factor
K_{fs}	static fracture intensity factor
K_{cl}	closure stress intensity factor
K_{max}	maximum stress intensity factor
K_{min}	minimum stress intensity factor
K_{op}	opening stress intensity factor
m	exponential of Paris equation
P	load
P_{max}	maximum load
P_{min}	minimum load
R	stress ratio, the ratio of the minimum value to the maximum value of cyclic stress
R_v	the ratio of the minimum load to the maximum load during the variable amplitude load process
v	crack opening displacement
W	width of CT specimen
da/dN	fatigue crack growth rate
γ_y	crack tip plastic radius
Δa	amount of crack growth
ΔK	range of stress intensity factor
ΔK_{eff}	range of effective stress intensity factor
ΔK_{op}	range of opening stress intensity factor
ΔK_{th}	threshold range of the crack growth stress intensity factor
ΔP	range of load
$\Delta\sigma$	range of stress
$\Delta\sigma_{eff}$	range of effective stress
ε	strain
σ	stress
σ_{max}	maximum stress
σ_{min}	minimum stress

References

1. Donachie, M.J.; Donachie, S.J. *Superalloys: A Technical Guide*; ASM International: Almere, The Netherlands, 2002.
2. Kishi, N.; Hasan, R.; Chen, W.; Goto, Y. Study of Eurocode 3 steel connection classification. *Eng. Struct* **1997**, *19*, 772–779. [CrossRef]
3. ANSI WEBSTORE. Available online: https://webstore.ansi.org/standards/bsi/bs76082014 (accessed on 8 November 2023).
4. Hobbacher, A. The development of the new IIW fatigue recommendations. In Proceedings of the IIW Ont. Conference on Performance of Dynamically Loaded Welded Structures, San Francisco, CA, USA, 14–15 July 1997.
5. Balasubramanian, T.; Balasubramanian, V.; Manickam, M.M. Fatigue crack growth behavior of gas tungsten arc, electron beam and laser beam welded Ti–6Al–4V alloy. *Mater. Des.* **2011**, *32*, 4509–4520. [CrossRef]
6. Guo, Y.; Chen, F.; Li, M.; Yu, H.; Li, W.; Deng, H. The effect of defect characteristics on prediction of fatigue life of TC4 titanium alloy welded joints. *Metals* **2023**, *13*, 1540. [CrossRef]
7. Liu, J.; Chen, J.; Sun, Z.; Zhang, H.; Yuan, Q. A study on fatigue crack closure associated with the growth of long crack in a new titanium alloy. *Metals* **2023**, *13*, 1377. [CrossRef]
8. Wang, Y.; Ma, H.; Zhang, Y.J. Fatigue crack growth behavior for gas tungsten arc welded joint of TC2 titanium alloys sheets. *Mater. Sci. Eng. A* **2023**, *881*, 145385. [CrossRef]
9. Emadinia, O.; Guedes, A.; Tavares, C.J.; Simões, S. Joining alumina to titanium alloys using Ag-Cu sputter-coated Ti brazing filler. *Materials* **2020**, *13*, 4802. [CrossRef]
10. Wang, Y.; Hu, B.; Wei, Y.; Feng, G.; Deng, D. Microstructure and mechanical properties of vacuum diffusion bonded Ti2AlNb/Ti/TC4 joint. *Crystals* **2021**, *11*, 770. [CrossRef]

11. Vishnuvardhan, S.; Murthy, A.R.; Choudhary, A. A review on pipeline failures, defects in pipelines and their assessment and fatigue life prediction methods. *Int. J. Press. Vessel. Pip.* **2022**, *201*, 104853. [CrossRef]
12. Su, M.; Xu, L.; Peng, C.; Han, Y.; Zhao, L. Fatigue short crack growth, model and EBSD characterization of marine steel welding joint. *Int. J. Fatigue* **2022**, *156*, 106689. [CrossRef]
13. Darveaux, R. Effect of simulation methodology on solder joint crack growth correlation and fatigue life prediction. *J. Electron. Packag.* **2002**, *124*, 147–154. [CrossRef]
14. Kang, H.T. Fatigue prediction of spot welded joints using equivalent structural stress. *Mater. Des.* **2007**, *28*, 837–843. [CrossRef]
15. Socie, D.F. Fatigue-life prediction using local stress-strain concepts: The primary emphasis of this paper is on the mechanics of a computer algorithm for cumulative fatigue damage. *Exp. Mech.* **1977**, *17*, 50–56. [CrossRef]
16. Wheeler, O.E. Spectrum loading and crack growth. *J. Basic Eng.* **1972**, *D94*, 181–186. [CrossRef]
17. Liu, X.; Wu, Q.; Su, S.; Wang, Y. Evaluation and prediction of material fatigue characteristics under impact loads: Review and prospects. *Int. J. Struct. Integr.* **2022**, *13*, 251–277. [CrossRef]
18. Neto, D.; Borges, M.; Antunes, F.; Jesus, J. Mechanisms of fatigue crack growth in Ti-6Al-4V alloy subjected to single overloads. *Theor. Appl. Fract. Mech.* **2021**, *114*, 103024. [CrossRef]
19. Sanaei, N.; Fatemi, A. Defect-based fatigue life prediction of L-PBF additive manufactured metals. *Eng. Fract. Mech.* **2021**, *244*, 107541. [CrossRef]
20. Willenborg, J.; Engle, R.; Wood, H. *A Crack Growth Retardation Model Using an Effective Stress Concept*; TM-71-1-FBR; Air Force Flight Dynamics Lab.: Dayton, OH, USA, 1971.
21. Ferreira, F.F.; Neto, D.M.; Jesus, J.S.; Prates, P.A.; Antunes, F.V. Numerical prediction of the fatigue crack growth rate in SLM Ti-6Al-4V based on crack tip plastic strain. *Metals* **2020**, *10*, 1133. [CrossRef]
22. Paris, P.C.; Erdogan, F. A critical analysis of crack propagation laws. *J. Basic Eng.* **1963**, *D85*, 528–534. [CrossRef]
23. Forman, R.G.; Kearney, V.E.; Engle, R.M. Numerical analysis of crack propagation in cyclic-loaded structures. *J. Basic Eng.* **1967**, *D89*, 459–464. [CrossRef]
24. Elber, W. *Fatigue crack propagation: Some effects of crack closure on the mechanism of fatigue crack propagation under cyclic tension loading*; University of New South Wales: Sydney, Australia, 1968.
25. Austen, I.; Walker, E. Corrosion fatigue crack growth rate information for offshore life prediction. *Steel Mar. Struct.* **1987**, *87*, 859–870.
26. Huang, C.-D.; Hwang, J.-R.; Huang, J.-Y. Optimization of vacuum brazing process parameters in Ti-6Al-4V alloy. *Metals* **2022**, *12*, 974. [CrossRef]
27. *ASTM E647-15e1*; Standard Test Method for Measurement of Fatigue Crack Growth Rates. ASTM Intertional: West Conshohocken, PA, USA, 2015.
28. Stephens, R.-I.; Fatemi, A.; Stephens, R.-R.; Fuchs, H.-O. *Metal Fatigue in Engineering*, 2nd ed.; Wiley-Interscience: New York, NY, USA, 2001; pp. 288–289.
29. Bannantine, A.; Socie, D. A Multiaxial Fatigue Life Estimation. *ASTM Int.* **1992**, *1122*, 249.
30. Hwang, J.-R. *Process Optimization and Fatigue Properties of Vacuum-Brazed Titanium Alloy*; National Science and Technology Council: Taipei, ROC, 2018.
31. Bannantine, J.A.; Comer, J.J.; Handrock, J.L. *Fundamentals of Metal Fatigue Analysis*; Prentice Hall: Englewood Cliffs, NJ, USA, 1990.
32. Elber, W. *The Significance of Fatigue Crack Closure.*; ASTM Intertional: West Conshohocken, PA, USA, 1971; pp. 230–242.
33. Schijve, J. *Fatigue of Structures and Materials*; Springer: Dordrecht, The Netherlands, 2009; pp. 209–256.
34. Mughrabi, H. ASM Handbook, Volume 19, Fatigue and Fracture. *ASM Int.* **1998**, *153*, 76.
35. Sullivan, A.; Crooker, T. Analysis of fatigue-crack growth in a high-strength steel—Part I: Stress level and stress ratio effects at constant amplitude. *J. Press. Vessel Technol.* **1976**, *98*, 179–184. [CrossRef]
36. Chen, H.; Yang, F.; Wu, Z.; Yang, B.; Huo, J. A nonlinear fatigue damage accumulation model under variable amplitude loading considering the loading sequence effect. *Int. J. Fatigue* **2023**, *177*, 107945. [CrossRef]
37. Beden, S.; Abdullah, S.; Ariffin, A.; Al-Asady, N. Fatigue crack growth simulation of aluminum alloy under spectrum loadings. *Mater. Des.* **2010**, *31*, 3449–3456. [CrossRef]

Disclaimer/Publisher's Note: The statements, opinions and data contained in all publications are solely those of the individual author(s) and contributor(s) and not of MDPI and/or the editor(s). MDPI and/or the editor(s) disclaim responsibility for any injury to people or property resulting from any ideas, methods, instructions or products referred to in the content.